

Research article

The influence of Dunlop and air microbubbling manufacturing methods on the physical, microstructural and mechanical properties of nano-alumina filled natural rubber latex foam

Amin Raveshtian, Mohammad Fasihi^{*}, Reza Norouzbeigi, Sajad Rasouli

School of Chemical Engineering, Iran University of Science and Technology (IUST), P.O. Box 16844–13114, Tehran, Iran

Received 21 December 2021; accepted in revised form 7 March 2022

Abstract. The impacts of nano-alumina (NA) as a filler and the manufacturing methods of Dunlop and air microbubbling on the physical, microstructural and mechanical properties of natural rubber latex foam (NRLF) were comprehensively investigated. The achieved crosslink density through the swelling method using the Flory–Rehner equation showed that the nano-alumina led to an increase in the crosslinking level in the foam. The foams prepared by the air microbubbling (BLF) had crosslink density 57–160% more than Dunlop (LF). Despite the fact that the nano-alumina enhanced the cell size and broadened their diameters probability distribution, the field-emission scanning electron microscopy illustrated that the air microbubbling resulted in the foams with 105% smaller cell size (0.113 mm) and 840% higher cell density ($57.94 \cdot 10^5$ cell/mm³). In addition, the calculated specific tensile strength, modulus, toughness, and elongation at break proved that the metallic oxide filler of nano-alumina improved the tensile characteristics of the NRLF up to 60%. According to the results, adding 3 phr nano-alumina to the foam increased the compression recovery to 86 and 99.4% in the LF and BLF samples, respectively. Finally, the analysis of variance was performed to optimize the formulation of foams prepared by two manufacturing methods.

Keywords: rubber, foam, Dunlop, microbubble, microstructure

1. Introduction

Natural rubber latex (NRL) is a stable aqueous medium containing particles of polyisoprene isomers that originated from the rubber tree (*Hevea brasiliensis*) in Brazil [1, 2]. This colloidal solution has many applications in various industrial and medical fields because of its fantastic properties, *e.g.*, high flexibility, elasticity, and strength [3]. In the last decades, NRL has been used to manufacture latex foam (NRLF) which has been considered as an economical material with favorable features, *e.g.*, buoyancy, thermal and acoustic insulation, lightweight, high porosity, good aging, and inertness properties [4]. Recently,

cushioning performance has attracted the attention of many polymer researchers because of the porous structure of NRLF, which can be used in car seats and furniture, pillows, mattresses, *etc.* [5]. This latex foam was manufactured using concentrated NRL presented by Schidrowitz and Goldsbrough [6] in 1914. Natural rubber latex foam is a cellular rubber that is produced by compounding NRL with some other chemical substances under different conditions [7]. In various industries, foams with good mechanical, microstructural and physical properties are required. Accordingly, different reinforcements such as fillers, *e.g.*, TiO₂ [8], calcium carbonate [9], carbon [10],

^{*}Corresponding author, e-mail: mfasihi@iust.ac.ir
© BME-PT

silicate [11], kenaf [12], and cellulose [13] have been added to the latex before foaming. The reinforcements have been used because the NRLF does not typically meet the requirement for industrial applications [13]. For example, Lee *et al.* [10] evaluated the influence of carbon black loading content on the mechanical properties of NRLF. Their results demonstrated that raising the carbon black content in the latex compound gradually led to the increment of the tensile strength and modulus of NRLF. Phomrak *et al.* [13] showed that the cellulose nanoparticles as filler for NRLF caused the improvement in the modulus, tensile strength and crosslink density of the foam. Prasopdee *et al.* [14] proved that using silica nanoparticles increased the compressive properties of the NRLF foam. Karim *et al.* [15] used kenaf powder to promote the mechanical and physical characteristics of the NRLF. Their resultant data indicated that the enhancement of kenaf content in the latex matrix reduced the elongation at break, tensile and compressive strength of the NRLF. In spite of the performed research on NRLF, the foam properties such as microstructural properties, tensile and compressive properties can be further improved in order to achieve the most economical and efficient NRLF [12, 16].

In addition to the amount and type of fillers, the producing method of NRLF also affects the properties of the foam [16]. The Dunlop method is a well-known process to manufacture latex foam, which was presented by Ramasamy *et al.* [17]. Despite the Dunlop method, Talalay is also used to produce latex foam as another method. Talalay leads to considerably soft foams with better cellular structure and flexibility compared to Dunlop [18]. Whereas using a high-speed mixer in the Dunlop process leads to large bubbles, which causes breakdown of the cell walls and reduces foam properties. [19–21]. Despite these two methods, many other manufacturing processes have also been introduced to produce the NRLF, but none were successfully accepted in the foam industries [16]. So far, new innovative ways have been developed to produce natural rubber latex foams. For example, Zhan *et al.* [22] manufactured a natural rubber latex foam composite filled with graphene oxide by vulcanizing the prepared hydrogel. In another study, they also made a natural rubber latex composite foam containing carbon nanotubes using a multi-step method [23]. Sirikulchaikij *et al.* [18] have recently introduced a method called air microbubbling for the production of natural rubber latex foams,

which can be an efficient alternative for the manufacturing method of these foams in the industries. Fillers have been used in natural rubber latex for proper purposes. For example, in the study of Zhan *et al.* [24], they used graphene to enhance the mechanical properties of the latex matrix and used it to increase the electrical conductivity of the composite. Zhan *et al.* [25] also investigated the effect of thermal and electrical conductivity of carbon nanotubes on the latex matrix in another study. In this work, nano-alumina (Al_2O_3) with diverse loading contents was used to improve mechanical and microstructural properties, crosslink density and physical features of NRLF. One of the most important properties of nano-alumina is its high thermal conductivity, which can distribute heat evenly in the matrix media and affect the curing properties. Based on our knowledge, this nanoparticle has never been used in natural rubber latex foams before. In addition, the effect of manufacturing methods of Dunlop and air microbubbling on the microstructure and mechanical properties of composite foams were also compared.

2. Materials and methods

2.1. Materials

High ammonia natural rubber latex (H-NRL) containing 60% dry rubber content (DRC) was bought from Zarm Scientific & Supplies Sdn. Bhd., Malaysia. The chemical substances for NRL compounding, *i.e.*, sulfur (S), zinc diethylthiocarbonate (ZDEC), phenolic type antioxidant (Wingstay L), potassium oleate (K-oleate), zinc oxide (ZnO), tetramethylthiuram disulfide (TMTD), sodium silicofluoride (SSF), diphenylguanidine (DPG) were supplied by Zarm Scientific & Supplies Sdn. Bhd., Malaysia. Also, nano-alumina (NA) were purchased from local company of RASA Co. (Esfahan, Iran) with a particle size of 50–100 nm, purity of 99.9% and the density of 3.98 g/cm^3 (grade: RS-Al- α).

2.2. Preparation of nano-alumina filled natural rubber latex foam

2.2.1. Dunlop method

The Dunlop method can be both a discontinuous process and a continuous process. Like any other rubber product, a proper formulation must be used to achieve a useful product. Basically, this formulation consists of 4 parts, namely latex base, foaming agent, gelling agent and curing agent. In this method (discontinuous), after preparing the latex compound, a

mixer is used to create bubbles inside the latex mixture. The gelling agent is then added to the mixture to maintain the shape of the foam, and followed by the foam is transferred into the mold and cured. In the beginning, the H-NRL was filtered and then the required amounts of the latex and the other chemical substances were weighed according to the formulation presented in Table 1. The filtered H-NRL was first stirred using a mechanical stirrer for half an hour. Then, sulfur was added to the latex and the compound was stirred for another 10 min. In the next step, ZDEC and TMTD as accelerators were slowly added to the latex mixture under mixing for 10 min. After the mixing process, phenolic-type antioxidant and NA powder were added to the mixture, respectively. Next, K-oleate as a surface-active and stabilizing agent was slowly added to the compound, which was continuously being stirred for 5 min at room temperature. This step is called maturation. During this process, the latex mixture was severely mixed for 5 min in order to increase the volume of the mixture to three times the original volume. After the foam had been reached the desired volume, the speed of the stirrer was reduced to obtain a uniform foam. The ZnO as activating agent and DPG as an accelerating agent was added to the foam for 1.5 min under beating. It should be noted that ZnO and DPG together act as primary gelling agents. After the primary gelling agent, SSF as the secondary gelling agent was also added to the foam during the beating for the same period of 1.5 min. The un-gelled mixture was poured into a prefabricated aluminum mold (at the ambient temperature), and the foam was allowed to gel at the ambient temperature for 3 min. Finally, the gelled foam was cured in a hot air oven at 105 °C

for 130 min. After the curing process, the vulcanized foam was removed from the mold and washed with distilled water to remove any remaining chemicals. In the end, the achieved NRLF-NA was dried in a hot air oven for 9 h at 70 °C to obtain a white foam.

2.2.2. Air microbubbling method

The preparation of latex foam in the air microbubble method was similar to the Dunlop process presented in Section 2.2.1, except for the foaming step. In this method, the foaming process involves the formation of bubbles inside the latex mixture poured into the bubble column by passing airflow created by an air compressor through a diffuser. The airflow is spread inside the column filled with latex mixture to increase the volume of the mixture. Then, like the Dunlop method, foam is poured into the mold and cured. The used formulation for the materials in the latex compound to make NRLF-NA via using the air microbubble method was according to Table 1 as well. In this manufacturing method, a laboratory device was designed in order to foam the latex compound, which was schematically exhibited in Figure 1. As shown in the figure, the required airflow for the foaming process was supplied by a compressor with a maximum output capacity of 50 cm³/min. The air compressor was connected to a vertical glass column with the best fitting size secured by a holding clamp. The flow rate of the air is adjustable by a valve connected to the compressor, which is monitored with a flow meter. After passing through the diffuser embedded in the bottom of the glass column, the airflow creates bubbles within the latex compound filled inside the column and turns it into foam.

In the foaming step, the first gelling agent of ZnO + DPG was quickly added to the latex mixture after the maturation. Then, a standing mixer with a dispersing impeller was used to mix the latex mixture for 45 s at high speed. Afterward, the second gelling agent of SSF was immediately added to the mixture under the mixing condition for another 45 s. It should be mentioned that the mixing process was performed so that no bubbles form in the latex mixture. Next, the latex was quickly poured into the glass column, and the airflow rate was set at 10 cm³/min. In this step, the bubbling process was rapidly performed in the latex mixture filled inside the glass column for 45 s in order to turn the mixture into foam. Followed by the un-gelled foam was rapidly poured into the aluminum mold at the ambient temperature,

Table 1. Formulation of NRLF compound filled with nano-alumina (NRLF-NA).

Ingredients	Total solid content, TSC [%]	Amount [phr]
H-NRL	60	100
S	50	2.2
ZDEC	50	0.9
TMTD	50	0.9
Antioxidant	50	1.0
SSF	25	1.2
K-oleate	20	3.0
DPG	40	0.3
ZnO	50	3.0
NA	100	0, 1, 2, 3



Figure 1. Schematic of the designed laboratory device for the manufacturing of NRLF-NA in the air microbubbling method.

and after the gelling process, it was cured, similar to the Dunlop method. Then, the vulcanized NRLF-NA was washed and dried according to the presented method in the previous section.

2.3. Testing performed on nano-alumina filled natural rubber latex foam

2.3.1. Density measurement

The density of the cured foam is calculated by the equation of: dividing the sample mass by its volume. The density was achieved based on an average of the five different specimens.

2.3.2. Swelling test

The swelling method at room temperature was applied according to ASTM D471, in order to determine the crosslinking degree of the cured NRLF-NA based on an average on the five different specimens. First, the vulcanized foam was cut into the volume of $2 \times 2 \times 0.6 \text{ cm}^3$ and followed by was weighed. Afterward, the samples were immersed into toluene for 48 h. After this period, the weight of the swelled samples was again obtained. The crosslink density can be obtained based on the samples weights after (m_i) and before (m_p) of the 48 h.

2.3.3. Field-emission scanning electron microscopy

Field-emission scanning electron microscopy (FSEM) (FSEM; FEI Inspect F, FEI Company, Hillsboro, Oregon, USA) image was taken from the cross-section surface of the vulcanized foam using an accelerating voltage of 10 kV. The foam sample was first frozen in liquid nitrogen, then broken and followed by vacuum-dried. Before observation, the sample was coated with a thin layer of gold.

2.3.4. Tension test

In order to perform the tensile test on the cured foam, Instron 3366 universal testing machine was used according to ASTM D412. Five dumbbell-shaped specimens (for averaging the results) were cut from the NRLF-NA using a Wallace die cutter. The tensile test was carried out at 23°C and a crosshead speed of 500 mm/min. This test was implemented to obtain the tensile properties, *i.e.*, tensile strength, elongation at break and tensile modulus, for the latex foam.

2.3.5. Compression test

The compression test for the cured latex foam was implemented according to ASTM D3574. First, five

specimens (for averaging the results) with the dimensions of 50 mm (length) by 50 mm (width) by 25 mm (height) were cut. The samples were placed between the two plates of the machine and compressed to 50% of their original thickness. Next, the samples were subjected to heat with the temperature of 70 °C in a hot air oven for 22 h. At the end of this period, the samples were allowed to rest for 30 min at the ambient temperature, and the final thickness of the samples was measured after the recovery. The compression set and recovery percentage can be calculated via using the initial, final, and space bars thicknesses of the samples.

3. Results and discussion

In this work, the resultant data was discussed with respect to the effects of the NA loading content and the manufacturing methods of Dunlop/air microbubbling on the physical, microstructural and mechanical properties of the NRLF-NA. The foam samples prepared by the Dunlop and air microbubbling methods were symbolized by LF x and BLF x , respectively, in which x is the NA content in phr, *i.e.*, LF0, LF1, LF2 and LF3, and BLF0, BLF1, BLF2 and BLF3.

3.1. Physical properties

3.1.1. Foam density

Densities of the LF x and BLF x samples at different x are shown in Figure 2. As seen, the air microbubbling method led to the enhancement of the foam density in the absence of NA particles compared to the Dunlop method. It can be attributed to the larger

cells in the LF0 sample compared to the BLF0. The NRLF-NA samples prepared by the Dunlop method had a higher density than the air microbubble. Generally, the foam density was increased with the loading content of NA in the LF x samples, and the furthest density belonged to the LF3. In fact, the nano-alumina particles may have affected the cell wall thickness and the size of bubbles created in the foam matrix. In the air microbubbling manufacturing method, the filler content in the range of 1–2 phr caused the reduction of the density of the foam, while the sample containing 3 phr of NA had the highest density.

According to the drastic effects of the latex foam microstructure on the physical properties of the foam [18], the consideration of LF x and BLF x samples from the microstructural aspect can be helpful to find the origin of the variations.

3.1.2. Crosslink density

Crosslink density is known as one of the most important parameters in the characterization of vulcanized elastomers [26, 27]. Most of the NRLF features, *e.g.*, physical, microstructural and mechanical properties, are strongly dependent on the crosslinking level of the foam [13]. Moreover, this characteristic is an essential parameter to examine the lattice structure of the latex foam [28, 29]. The crosslink density of the LF x and BLF x samples at different amounts of x were calculated using the swelling method according to Flory–Rehner equation (FR) as Equations (1)–(4) [30–32]:

$$x_p = \frac{m_p}{m_t} \quad (1)$$

$$V_p = \frac{\frac{x_p}{\rho_p}}{\frac{x_p}{\rho_p} + \frac{1-x_p}{\rho_s}} \quad (2)$$

$$-\left[\ln(1 - V_p) + V_p + \chi V_p^2\right] = \frac{\rho V_0 V_p^{1/3}}{M_c} \quad (3)$$

$$CD = \frac{1}{5M_c} \quad (4)$$

where x_p demonstrates the mass fraction of polymer, which was obtained from the weights of the samples before (m_p) and after (m_t) the swelling process (see Section 2.3.2). The term of V_p illustrates the volume fraction of polymer in the swollen samples, and ρ , ρ_s and ρ_p are composite, toluene, and polymer densities, respectively. The terms of M_c and V_0 are physical

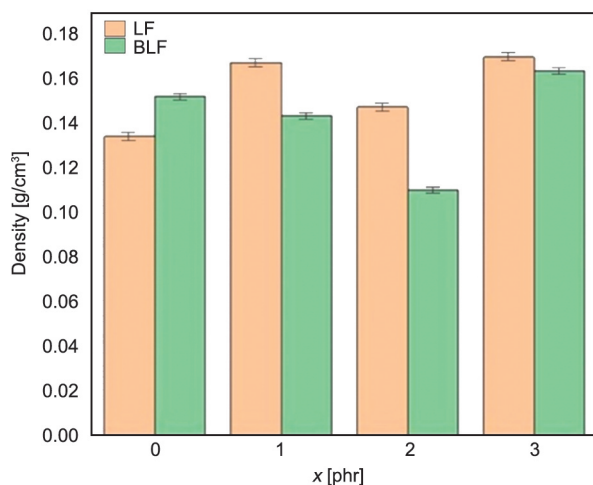


Figure 2. Density of the LF x and BLF x samples fabricated by the Dunlop and air microbubbling methods, respectively, as the function of the NA loading content, x .

crosslinking concentration and molar volume of toluene, respectively. The parameter of χ is the Flory–Huggins interaction parameter between toluene and natural rubber, which was reported 0.42 in the research work of Phomrak *et al.* [13]. Finally, the CD value (crosslink density) of the NA filled-NRLF was calculated from Equations (1)–(4), and the achieved results for the LFX and BLFX samples were summarized in Table 2. Adding 1 phr of nanoparticles to the latex foam reduced the crosslinking degree. In contrast, more amounts of filler caused the increment of the CD value. It can be attributed to the more uniform heat distribution in the latex compound during the curing process due to the presence of nano-alumina, a metallic oxide material with a high thermal conductivity [33]. This trend was the same in both LFX and BLFX samples. According to the table, the CD amount in the BLFX samples was much further than the LFX. It means that more crosslinking reactions occurred between the NR chains in the air microbubbling than the Dunlop method, resulting in a foam with a higher level of crosslinking. This phenomenon influences the microstructural and mechanical properties of the foam significantly because of the association of these features with the amount of CD . The crosslinking density results by themselves may not draw a clear conclusion, but they are a piece of a puzzle that unmask the effect of nano-alumina on the thermal, microstructural and mechanical properties of natural rubber latex foam. In this regard, we found a proper feature in the effect of nano-alumina on the thermal characteristics and kinetics of curing reaction of NRLF-NA in our previous work [34]. In fact, it was proved that the number of created covalent bonds to construct the network structure in NRLF-NA is a function of the NA amount. Virtually, The NA has a descendant effect on

the crosslinking amount of NRLF-NA and after $x = 1$ phr an ascendant impact. Therefore, $x = 1$ phr led to the lowest amount of crosslinking density in the LF1 sample. In fact, this behavior resulted from the decrease in the sulfurs diffusivity in the media due to an early evaporation of water and further solidification of the NRLF-NA [34]. Hence, the results of crosslinking density help to reveal the hidden insights about the mechanism of action in the NRLF-NA foams.

3.2. Microstructural properties

FSEM analysis was used to characterize the microstructure and cellular properties of the LFX and BLFX samples manufactured by the Dunlop and air microbubbling methods, respectively. The images with the $200\times$ magnification were taken from the cross-section of the samples to observe the arrangement, morphology, dispersion and size of the foam's cells. Moreover, the presence of cracks on the foam cell wall can be monitored by these FSEM images. Figure 3 shows the FSEM of the LFX and BLFX samples at $x = 0, 1, 2$ and 3 phr. It should be mentioned that Figure 3 shows only one of the taken images for each sample. According to the figure, the cavities on the cell wall of all the foam samples clearly indicate that the foam structure was open-cell [16] and the cells were connected to one another. As shown in Figure 3a₁, the cell size of the LF0 sample in the absence of the alumina nanoparticles was very large. There were many holes and cracks on their cell wall as well. The cell size and the holes on the cell wall were significantly reduced with the increment of the NA content. Nonetheless, the large cavities have still existed in some parts of the foam. In the LF2 sample, the cell size and the number of holes were increased compared to LF1, which caused many tears and cavities on the foam cell wall. More enhancement of the filler content in the foam almost did not change the cell size, while the number of the cavities on the cell wall were greatly decreased.

As seen in Figure 3b₁, the foam cells in the BLF0 sample were much smaller, denser and more regular, with fewer cavities than in the LF0 sample. This achievement explains the origin of the density difference between the LF0 and BLF0 samples presented in Figure 2 clearly. The addition of 1 phr nanoparticles increased the cell size, which led to the reduction of the cell order. This phenomenon caused the foam density decrement compared to the sample

Table 2. Crosslinking concentration (M_c) and density (CD) calculated according to the FR equation for the LFX and BLFX samples as the function of NA content (x).

Sample	M_c [m ³ /mol]	CD [mol/m ³]
LF0	0.1474	3.392
LF1	0.2060	2.402
LF2	0.1511	3.308
LF3	0.0543	9.195
BLF0	0.0936	5.341
BLF1	0.0978	5.112
BLF2	0.0576	8.667
BLF3	0.0343	14.566

without nanoparticles (see Figure 2). More increase in the x amount led to decreasing and raising the cell size in the BLF2 and BLF3 samples, respectively. According to Figures 3a and 3b, the cell shape in the

foam prepared by the microbubbling method was much more spherical than the samples made by the Dunlop process. This morphology can influence the mechanical properties of the foam significantly.

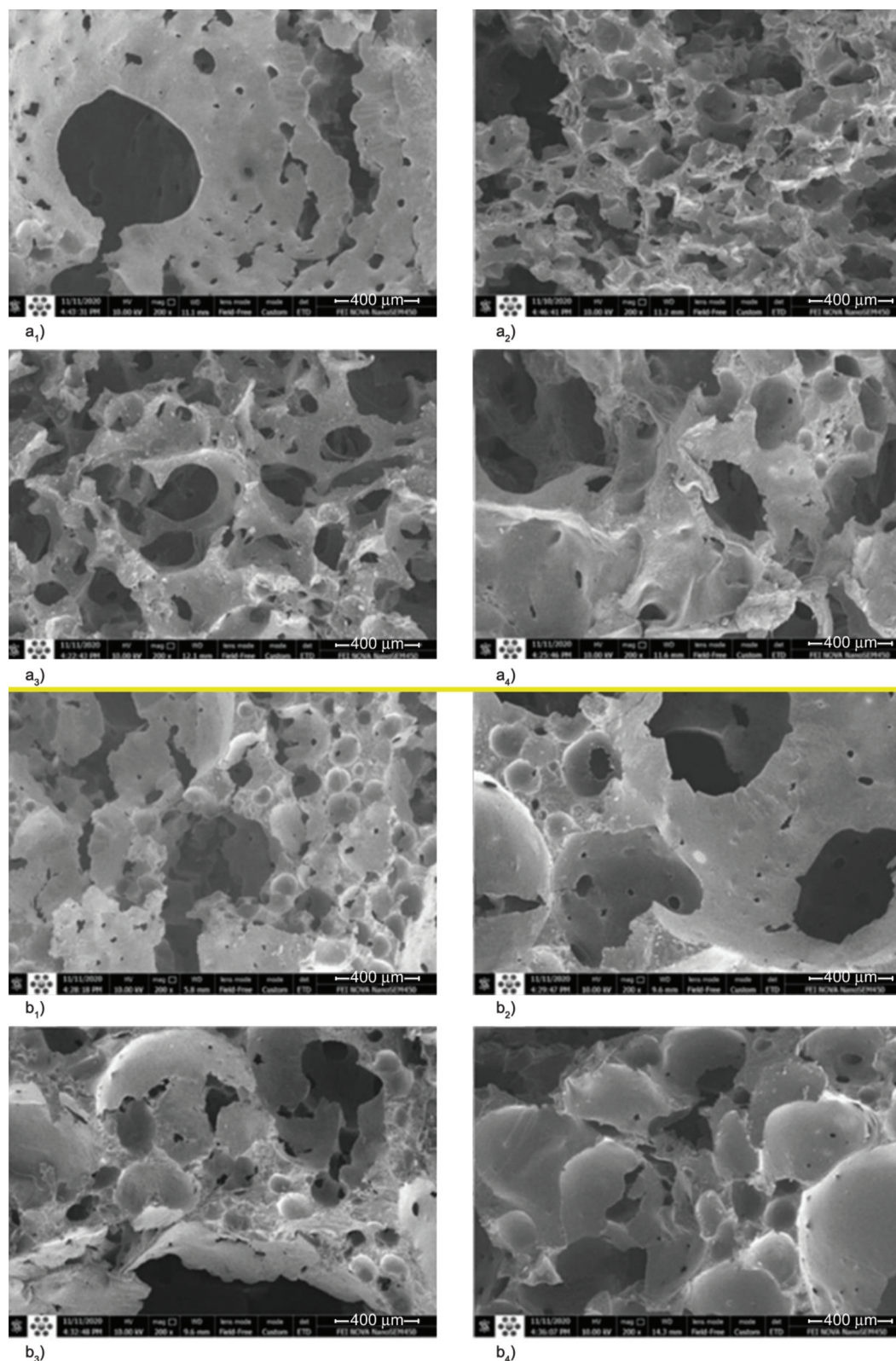


Figure 3. Field-emission scanning electron microscopy (FSEM) images with 200× magnification from the cross surface of (a₁–a₄) LFX and (b₁–b₄) BLFX samples with (a₁, b₁) $x = 0$, (a₂, b₂) $x = 1$, (a₃, b₃) $x = 2$ and (a₄, b₄) $x = 3$ phr nano-alumina particles.

Furthermore, to create a deep insight into the effects of the filler and the manufacturing methods on the microstructural characteristics of the foams, first, the diameter of the cells for each LFX and BLFX sample was obtained. This process was performed using the FSEM images of Figure 3. Then, the probability density function (PDF) of the cell diameters was calculated for all the foam samples. The achieved PDFs are shown in Figure 4 for the LFX and BLFX samples. As seen in the figure, increasing of 1 phr NA in the foam formulation prepared by the Dunlop method reduced the cell diameter and led to thinner distribution for the foam cell diameters. While, the cells diameter in the BLFX samples was increased with the loading content of NA. Similar to the LF1 sample, the BLF1 had thinner distribution for its cell diameters compared to the other BLFX.

Additionally, to quantitate the cell characteristics and as well as the PDF distributions presented in Figure 4, the average cell diameter (d_a) and the standard deviation (σ) of the results were calculated via the Equations (5) and (6) [35]:

$$d_a = \frac{1}{N} \sum_{i=1}^N d_i \quad (5)$$

$$\sigma = \sqrt{\frac{\sum_{i=1}^N (d_i - d_a)^2}{N - 1}} \quad (6)$$

In which d_i is the diameter of cell i th, and N is the number of measured cells to compute d_a for each foam sample. In this work, N was selected equal to 50.

Despite the cell size, two other important criteria in the foam microstructural characterization, *i.e.*, cell density (N_c) and the cell wall thickness (δ) were also calculated as Equations (7)–(9) [36]:

$$VER = \frac{NR \text{ density}}{\text{Foam density}} \quad (7)$$

$$N_c \cong \frac{10^4}{d_a^3} \left[1 - \frac{1}{VER} \right] \quad (8)$$

$$\delta = d_a \left[\frac{1}{\sqrt{1 - \frac{1}{VER}}} - 1 \right] \quad (9)$$

The parameters of VER and NR density are the volume expansion ratio and density of natural rubber, respectively. The calculated cell characteristics for each LFX and BLFX sample are summarized in Table 3. As seen in the table, the cell size was reduced with adding 1 phr NA to the LFX foam, while more increment of the filler had a vice versa effect. This issue caused the highest N_c for the LF1 compared to the other LFX samples. Also, the δ value was ascendant with the increment of the filler content. In conjunction with the BLFX samples, the nano-alumina led to increasing the d_a amount of the foam. In general, the

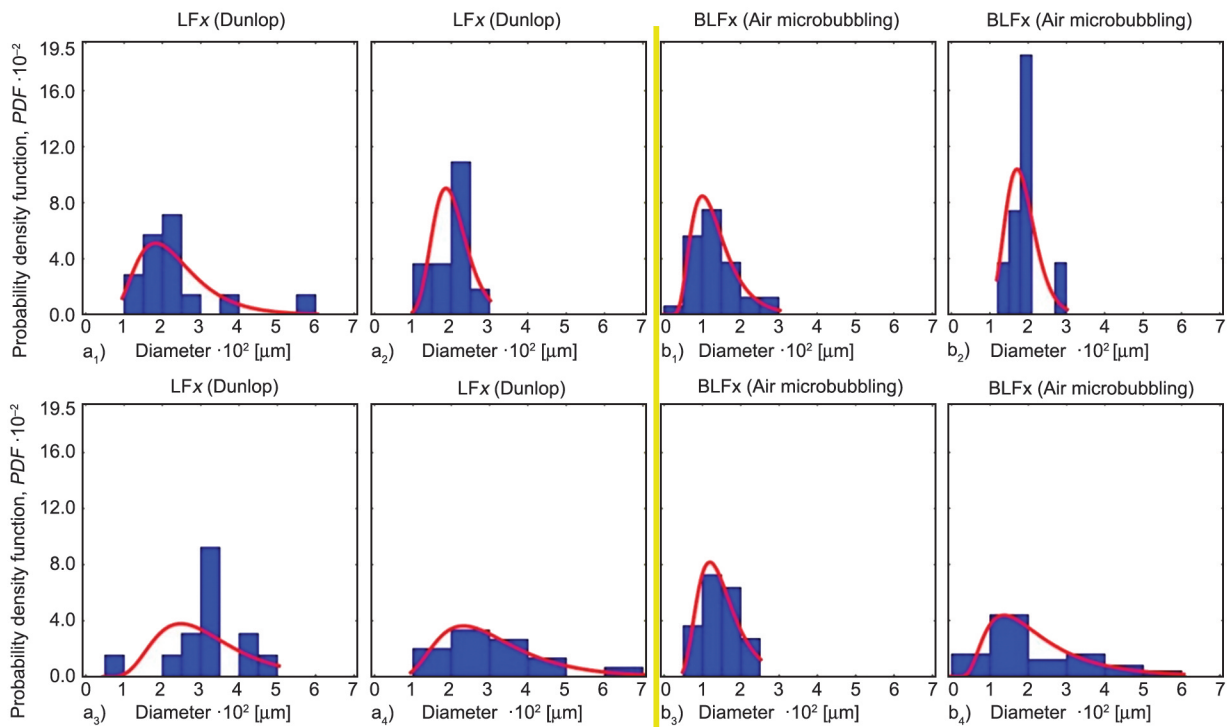


Figure 4. Probability density function (PDF) of the cell diameters for the LFX (a₁–a₄) and BLFX (b₁–b₄) samples with (a₁, b₁) $x = 0$, (a₂, b₂) $x = 1$, (a₃, b₃) $x = 2$ and (a₄, b₄) $x = 3$ phr, respectively.

Table 3. Microstructural characteristics of the LFX and BLFX samples at different amount of x (nano-alumina content in phr). The parameters of d_a , σ , N_c and δ are the average cell diameter, standard deviation, cell density and the cell wall thickness, respectively.

Sample	$d_a \pm \sigma$ [mm]	N_c [cell/mm ³]	δ [mm]
LF0	0.232±0.112	6.84·10 ⁵	0.0188
LF1	0.201±0.042	10.10·10 ⁵	0.0210
LF2	0.314±0.093	2.71·10 ⁵	0.0284
LF3	0.309±0.132	2.76·10 ⁵	0.0328
BLF0	0.113±0.054	57.94·10 ⁵	0.0105
BLF1	0.183±0.042	13.79·10 ⁵	0.0160
BLF2	0.148±0.049	27.17·10 ⁵	0.0096
BLF3	0.226±0.125	7.13·10 ⁵	0.0230

NA decreased and enhanced the cell density and cell wall thickness in the BLFX samples, respectively, except BLF2. The calculated microstructural features of the latex foams have a good agreement with the FSEM and the PDF curves results presented in Figure 3 and Figure 4, respectively. According to Table 3, the average cell diameter and its standard deviation in the BLFX samples was much lower than the LFX samples. Therefore, the preparation of the NRLF-NA with the air microbubbling method improved the microstructural characteristics of the latex foam.

In order to unmask the mechanism of action of nano-alumina in the LFX and BLFX samples, the FSEM images with the 6000–30 000× magnification were taken from the cell wall surface of the foams. These FSEMs can help to observe the nanoparticles attachment to the cell wall, the presence of cracks and cavities on the wall and the quality of the filler dispersion. Figure 5 show the FSEM images taken from the cell wall surface of the LFX and BLFX samples, respectively.

As seen in Figure 5a₁, the image with a magnification of 30 000 times from the LF0 sample showed the cell wall with a clean surface without the presence of the NA particles. However, very small particles were visible on the surface that could possibly be the remaining unreacted chemicals in the foam composition (even after the washing process of the cured foam). Also, there were very small cracks on the cell wall. The FSEM image with the magnification of 24 000× from the cell wall of the LF1 sample (Figure 5a₂) exhibited a good dispersion of the nano-alumina particles in the foam matrix. Nonetheless, there were nanoparticles aggregates in some parts of

the image. The average size of these aggregated particles was about 1–3 μm. The cracks were also observed on the cell wall, which were slightly larger than the LF0 sample. The 6000× image from the LF2 cell wall indicated clearly that despite the well-dispersed nanoparticles in the media, there were some aggregates in different parts of the FSEM with an average diameter of about 5–8 μm. While there were no cracks or holes on the foam cell wall. According to the 12 000× FSEM presented in Figure 5a₄, the size of the aggregated nanoparticles in the LF3 was significantly decreased to 1–2 μm with good dispersion in the foam matrix. Also, the high thickness and layers of the cell wall were clearly observed, which can improve the mechanical properties of this sample.

Figures 5b₁–5b₄ exhibits the 6000–12 000× FSEM images taken from the cell wall of the BLF0, BLF1, BLF2 and BLF3 samples, respectively. Similar to the LF0 sample, there were not any nanoparticles on the surface of the cell wall. In conjunction with the LF1 sample, it was seen that the nanoparticles were well attached to the cell wall. Nevertheless, the aggregates with a size of about 3–6 μm were observed. In spite of the good and thick cell wall without any cracks, very small cavities have existed on the surface. Increasing the filler loading content to 2 phr led to the inadequate dispersion for the nanoparticles and the large and significant cracks on the cell wall (see Figure 5b₃). This issue was the main factor for the existence of multiple ruptures in the cell wall and a significant drop in the density of this sample (see Figure 2). According to Figure 5b₄, the BLF3 sample had the thickest cell wall without any cracks and cavities compared to the other BLFX samples, like the LF3. However, some aggregates with an average size of 3–4 μm were observed in some parts of the surface.

3.3. Mechanical properties

3.3.1. Tensile properties

The stress-strain curves for the LFX and BLFX samples resulted from the tensile test are shown in Figure 6, respectively. The tensile characteristics, *i.e.*, tensile strength (TS), modulus (E), toughness (A) and elongation at break (S_{max}) for all the foam samples were extracted from Figure 6 and listed in Table 4. The mentioned mechanical characteristics are defined: TS : the maximum load that a material can support without fracture when being stretched, E : the stress divided by the strain, A : The area underneath

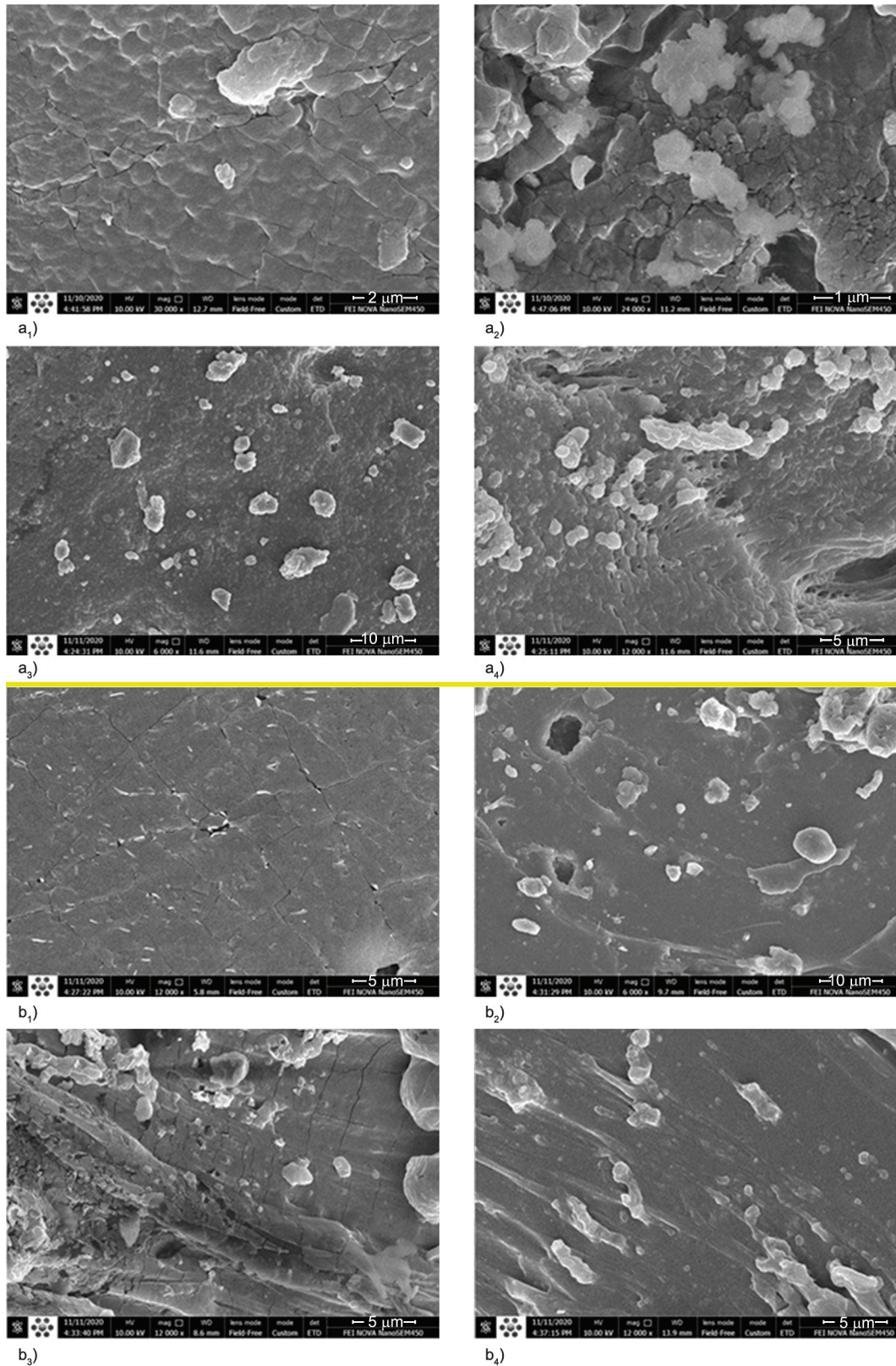


Figure 5. Field-emission scanning electron microscopy (FESEM) images with 6000–30 000 \times magnification from the cell wall surface of (a₁–a₄) LFX and (b₁–b₄) BLFX samples with (a₁, b₁) $x = 0$, (a₂, b₂) $x = 1$, (a₃, b₃) $x = 2$ and (a₄, b₄) $x = 3$ phr nano-alumina particles.

the stress–strain curve and S_{\max} : the ratio between the changed length and initial length after breakage of the test specimen, respectively. As seen in the table,

with increasing the NA amount from 1 to 3 phr, the TS value of the LFX foams was generally increased compared to the sample without nanoparticles. The

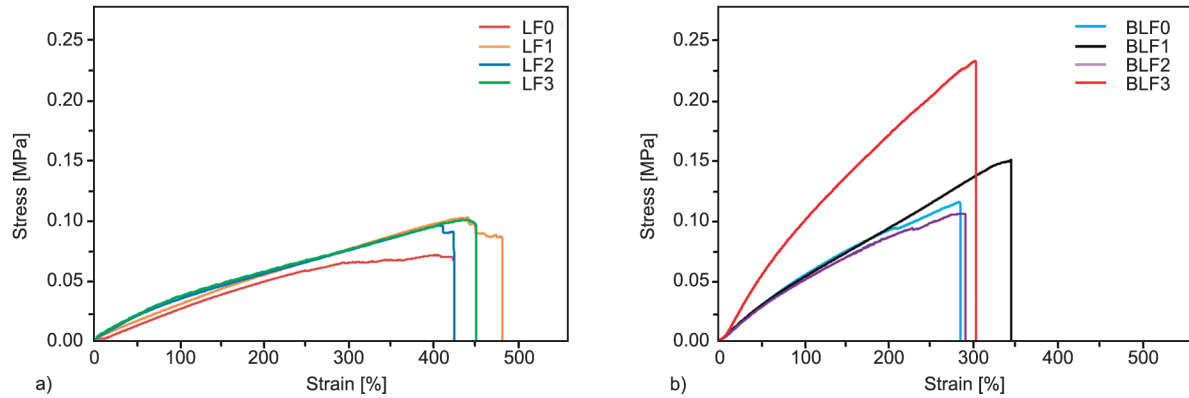


Figure 6. Stress-strain (tensile) curves of (a) LFX and (b) BLFX samples with different nano-alumina content, x .

TS value was almost the same in the LF1, LF2, and LF3 samples, which was 42% higher than the LF0 tensile strength. The variation trend of the modulus of the LFX sample was as similar as their TS trend. It can be seen that the E value of the LF1, LF2 and LF3 samples was increased by 35% compared to the LF0. The obtained results comply with this general rule; the E and TS values of a composite material increase with increasing the loading content of the reinforcing fillers [37, 38]. Similarly, the calculated A values for the LFX samples measuring the surface area below the stress-strain graphs showed that the nanoparticles increased the toughness of the foams generally. As expected, the LF1 sample had the highest amount of A . In fact, the enhancement of the cell wall thickness (see Table 3) and better cell dispersion (see Figure 3) with increasing the x amount were the main factors to improve the tensile properties of the LFX samples. Also, the increment of the LFX crosslink density (see Table 2) with raising the loading content of NA was another main reason for the promotion of the foam tensile characteristics. Because the CD level influences directly the E and TS values of crosslinked materials [39, 40].

Furthermore, to calculate the specific amounts of the tensile strength, modulus and toughness, *i.e.*, TS^* , E^* and A^* , the achieved TS , E and A values were divided into the density of the foam. The resulting data were summarized in Table 4 for all the samples as well. As listed in the table, the TS^* and E^* values for the LFX samples were ascendant with the filler content and after $x = 2$ phr descendant. This critical point was $x = 1$ phr for the specific toughness. The S_{max} value for the LFX samples was increased with increasing the amount of alumina nanoparticles, except for the LF2 sample, because the N_c amount in the LF2 was the least ($N_c = 2.71 \cdot 10^5$ cell/mm³) compared to the other LFX samples (see Table 3). In contrast, the S_{max} of the LF1 sample was the furthest because of its highest cell density of $10.10 \cdot 10^5$ cell/mm. Indeed, the enhancement of the d_a value of the cells (Table 3) and the presence of cell wall rupture in the LF2 samples led to the decrement of the foam elongation at break. Whereas this behavior was vice versa for the LF1 sample. In conjunction with the samples prepared by the air microbubbling method, the TS amount of the BLFX samples was increased with increasing the nanoparticle content, except the BLF2. The modulus and the

Table 4. The tensile characteristics of the LFX and BLFX samples. The parameters of TS , E , A and S_{max} are the tensile strength, modulus, toughness, and elongation at break, respectively.

Sample	TS [MPa]	E [MPa]	A [MPa]	TS^* [J/g]	E^* [J/g]	A^* [J/g]	S_{max} [%]
LF0	0.070	0.0170	0.1885	0.5196	0.1262	1.399	419.00
LF1	0.101	0.0230	0.2840	0.6033	0.1369	1.691	445.40
LF2	0.099	0.0231	0.2337	0.6707	0.1561	1.580	411.00
LF3	0.099	0.0225	0.2653	0.5810	0.1321	1.557	443.00
BLF0	0.116	0.0410	0.1935	0.7606	0.2680	1.268	283.70
BLF1	0.152	0.0460	0.2841	1.0560	0.3194	1.972	342.19
BLF2	0.105	0.0365	0.1885	0.9950	0.3293	1.701	286.60
BLF3	0.233	0.0770	0.3995	1.4200	0.4689	2.433	302.77

*indicates the specific values of the tensile characteristics.

toughness of the BLF x samples also have had a similar trend to the TS . According to Table 4, the trend of the tensile-specific characteristics of the BLF x samples was generally ascendant with the loading content of the nano-alumina. The slope of the variations for the samples made by the microbubbling method was more intensive than the Dunlop. In general, the tensile strength and modulus of the BLF x samples were generally higher than those of the LF x samples. This increase was significant for the BLF3; its TS value was increased 2.35 times compared to the LF3 sample (see Figure 6 and Table 4). The modulus of the BLF3 sample was also increased 3.42 times than the LF3 sample. Moreover, the obtained A and A^* values of the BLF x samples exhibited an incremental trend with x , except the BLF2 sample. As shown in Table 4, the amount of S_{max} for the BLF x samples was lower than the LF x specimens, because the air microbubbling method caused the foams with higher crosslink and cell densities than the Dunlop method (see Table 2 and Table 3). Similar to the LF1, the BLF1 sample also had the highest amount of S_{max} because of the lowest CD amount. Factually, the reduction of crosslinking degree at 1 phr increased the mobility of the rubber chains because of the fewer connections between the NR chains. This issue caused a more amount of the S_{max} in the LF1 and BLF1 samples.

3.3.2. Compression properties

The compression set (C_s) and recovery percentage (R) are two important criteria to quantitate the compression characteristics of the foams [41]. Table 5 shows the initial (L_0), underload (space bars thickness) (L_1) and final (L_2) lengths of the LF x and BLF x samples achieved from the compression test. According to the obtained L_0 , L_1 and L_2 , and the Equations (10) and (11) [1], the C_s and R amount for the latex foams were calculated and then were listed in Table 5.

$$C_s = \frac{L_0 - L_2}{L_0 - L_1} \cdot 100 \text{ [\%]} \quad (10)$$

$$R = \frac{L_2}{L_0} \cdot 100 \text{ [\%]} \quad (11)$$

As seen in Table 5, the C_s amount of the foams was increased with the NA loading content, and then the trend was changed after $x=2$ and $x=1$ phr for the LF x and BLF x samples, respectively. The reverse

Table 5. Compression characteristics of the LF x and BLF x samples. The terms of L_0 , L_1 and L_2 are the initial, underload and final lengths of the samples, respectively. The parameters of C_s and R indicate the compression set and recovery percentage, respectively.

Sample	L_0 [mm]	L_1 [mm]	L_2 [mm]	C_s [%]	R [%]
LF0	25	12.5	21.03	31.76	84.12
LF1	25	12.5	20.98	32.16	83.92
LF2	25	12.5	20.71	34.32	82.84
LF3	25	12.5	21.50	28.00	86.00
BLF0	25	12.5	22.75	18.00	91.00
BLF1	25	12.5	22.30	21.60	89.20
BLF2	25	12.5	22.90	16.80	91.60
BLF3	25	12.5	24.85	1.20	99.40

trend was observed for the recovery parameter of R . The resultant C_s and R values have good conformity with the obtained microstructural characteristics and the CD amounts (see Table 2 and Table 3) of the latex foams. In fact, the reduction of the CD level of the latex foam led to a weaker network structure. Subsequently, when the pressure was removed from the sample, the rubber chains returned to their former positions with a delay. This issue caused the enhancement of the compression set and the decrement of the R -value. In contrast, more increments of the NA nanoparticles raised the crosslink density (see Table 2) and changed the variation trend of the compression characteristics. It should be mentioned that the largest cell size ($d_a = 0.314$ mm) in the LF2 sample also had an undesirable effect on the foam compression features, which caused the highest C_s and the lowest R values. As seen in Table 5, the air microbubbling manufacturing method caused a much lower compression set and higher recovery for the NRLF-NA than the Dunlop method.

3.4. Analysis of variance

According to the vast amounts of data obtained, the physical, microstructural and mechanical achievements should be considered simultaneously to select the best LF x and BLF x sample with the most efficient content of NA. Accordingly, the results of analysis of variance (ANOVA) implemented by MINITAB®18 [36] were used to find the effective LF x and BLF x samples. ANOVA supplies the analysis of each calculated response to measure the statistical significance of the effect of nano-alumina on the physical, microstructural and mechanical characteristics of the latex foams. In this study, the significance of the NA

content, x , in the LFX and BLFX samples has been investigated to find its interaction on the responses. The basic characteristics of the foams, *i.e.*, foam density, d_a , σ , A^* and C_s were set as the responses because they are the origin of the behavioral variations in the foams. Also, the content of nano-alumina in the foam formulation, x , was applied as the variable. The fitted linear models provided by the numerical coefficients (with the perfect P -values [42]) for the properties of the LFX and BLFX samples resulting from the ANOVA were reported in Table 6. The coefficients of the presented equations in Table 6 illustrate the impact of the related term on that property. The negative and positive coefficient shows a decreasing and synergistic effect on the responses, respectively.

In order to find the best amount of filler for the LFX and BLFX specimens, an optimization process was carried out on the obtained equations (see Table 6). The objective of optimization was to minimize foam density, d_a , σ and C_s and maximize A^* , respectively, since these features are favorable for the foam industry [8]. The desirability function approach (D) was also used in the applied optimization process. In fact, this function is based on transforming each property into a desirability amount, combining the individual responses into a composite function and then its optimization [43]. The optimization process showed that the LF1 and BLF2 were the optimum samples with the desired properties, which had $D=0.982$ and $D=0.979$, respectively. Nonetheless, all the results in this work exhibited that the samples prepared by the air microbubbling method had more improved properties than the Dunlop.

4. Conclusions

The comparison of the LFX and BLFX densities indicated that the air microbubbling method generally

caused the foams with lower densities than Dunlop in the presence of the filler. In the LFX samples, the foam density was increased with increasing the loading content of NA, while the BLFX samples had a descendant and after $x = 2$ phr ascendant trend with x for their densities. The calculated crosslink density via using the swelling method and the Flory–Rehner equation illustrated that the presence of nano-alumina improved the strength of the network structure via increasing the foams CD amount. The variation of the crosslinking degree with the NA was incremental in both the methods of Dunlop and air microbubbling, except the foams with $x=1$ phr. However, the amount of CD for the BLFX samples was 57–160% more than the LFX specimens. Field-emission scanning electron microscopy showed that the cell structure of all the foams was open-cell, and the cell shape was different in the LFX and BLFX samples. The taken FSEM images from the cross surface of the samples indicated that the BLFX samples had more regular and spherical cells than the LFXs. Also, the air microbubbling process resulted in the foams with fewer cracks and cavities on their cell wall, and up to 840% higher cell density ($57.94 \cdot 10^5$ cell/mm³) and 105% smaller cell size (0.113 mm). The calculated tensile strength, modulus, toughness, elongation at break of the foams and as well as their specific values proved that the air microbubbling method improved the tensile characteristics of the latex foams much more than Dunlop. This improvement was up to 60% more than the well-known method of Dunlop. The addition of 3 phr nano-alumina led to the increment of the modulus and tensile strength of the BLF3 sample to 3.42 and 2.35 times of those in the LF3, respectively. The calculated compression set and recovery for the foams illustrated that the filler increased these features and then the trend was

Table 6. Linear model for the responses in the ANOVA consideration, where x is the NA content in phr.

Sample	Response	Linear model
LFX	Density	$= 0.1552 - 0.0205x[0] + 0.0127x[1] - 0.0073x[2] + 0.0151x[3]$
	d_a	$= 0.264 - 0.032x[0] - 0.063x[1] + 0.05x[2] + 0.0450x[3]$
	σ	$= 0.09475 + 0.01725x[0] - 0.05275x[1] - 0.00175x[2] + 0.03725x[3]$
	A^*	$= 1.557 - 0.1577x[0] + 0.1343x[1] + 0.02325x[2] + 0.00025x[3]$
	C_s	$= 31.56 + 0.20x[0] + 0.60x[1] + 2.760x[2] - 3.560x[3]$
BLFX	Density	$= 0.1429 + 0.009625x[0] + 0.001125x[1] - 0.03208x[2] + 0.02133x[3]$
	d_a	$= 0.1675 - 0.05450x[0] + 0.01550x[1] - 0.01950x[2] + 0.05850x[3]$
	σ	$= 0.06750 - 0.01350x[0] - 0.02550x[1] - 0.01850x[2] + 0.05750x[3]$
	A^*	$= 1.844 - 0.5755x[0] + 0.1285x[1] - 0.1425x[2] + 0.5895x[3]$
	C_s	$= 14.40 + 3.600x[0] + 7.200x[1] + 2.400x[2] - 13.20x[3]$

changed after $x = 1$ and $x = 2$ phr for the BLFx and LFx samples, respectively. According to the compression results, the LFx and BLFx samples had the compression set up to 28 and 1.2%, and the recovery percentage up to 86 and 99.4%, respectively. In the end, the LFx and BLFx foams with $x = 1$ and $x = 2$ phr of NA, respectively, were found as the most efficient foams with the desired properties for the foam industry via using the analysis of variance (ANOVA) of the calculated properties. The considerations in this work showed clearly that the air microbubbling method could be an efficient alternative for the Dunlop process. In addition, using metallic oxide filler of nano-alumina results in a NRLF with more improved properties compared to other used fillers due to increasing the heat distribution in the curing process because of the higher thermal conductivity of alumina.

References

- [1] Bashir A. S., Manusamy Y., Chew T. L., Ismail H., Ramasamy S.: Mechanical, thermal, and morphological properties of (eggshell powder)-filled natural rubber latex foam. *Journal of Vinyl and Additive Technology*, **23**, 3–12 (2017).
<https://doi.org/10.1002/vnl.21458>
- [2] Suksup R., Sun Y., Sukatta U., Smitthipong W.: Foam rubber from centrifuged and creamed latex. *Journal of Polymer Engineering*, **39**, 336–342 (2019).
<https://doi.org/10.1515/polyeng-2018-0219>
- [3] Naphon P., Wiriyaart S., Naphon N.: Thermal, mechanical, and electrical properties of rubber latex with TiO₂ nanoparticles. *Composites Communications*, **22**, 100449 (2020).
<https://doi.org/10.1016/j.coco.2020.100449>
- [4] Martins M. A., Moreno R. M., McMahan C. M., Brichta J. L., de S. Gonçalves P., Mattoso L. H. C.: Thermo-oxidative study of raw natural rubber from brazilian IAC 300 series clones. *Thermochimica Acta*, **474**, 62–66 (2008).
<https://doi.org/10.1016/j.tca.2008.06.001>
- [5] Kudori S. N. I., Ismail H., Shuib R. K.: Kenaf core and bast loading vs. properties of natural rubber latex foam (NRLF). *BioResources*, **14**, 1765–1780 (2019).
<https://doi.org/10.15376/biores.14.1.1765-1780>
- [6] Ramasamy S., Ismail H., Munusamy Y.: Effect of rice husk powder on compression behavior and thermal stability of natural rubber latex foam. *BioResources*, **8**, 4258–4269 (2013).
- [7] Mahathaninwong N., Chucheeep T., Karrila S., Songmuang W., Rodsang N., Limhengha S.: Morphology and properties of agarwood-waste-filled natural rubber latex foam. *BioResources*, **16**, 176–189 (2021).
<https://doi.org/10.15376/biores.16.1.176-189>
- [8] Seerod K., Sangjumba J., Seithtanabutara V.: Effect of bio-fibrils incorporating with TiO₂ on the properties of natural rubber foam. *Key Engineering Materials*, **718**, 26–29 (2016).
<https://doi.org/10.4028/www.scientific.net/KEM.718.26>
- [9] Cai H.-H., Li S.-D., Tian G.-R., Wang H.-B., Wang J.-H.: Reinforcement of natural rubber latex film by ultrafine calcium carbonate. *Journal of Applied Polymer Science*, **87**, 982–985 (2003).
<https://doi.org/10.1002/app.11410>
- [10] Lee E.-K., Choi S.-Y.: Preparation and characterization of natural rubber foams: Effects of foaming temperature and carbon black content. *Korean Journal of Chemical Engineering*, **24**, 1070–1075 (2007).
<https://doi.org/10.1007/s11814-007-0123-6>
- [11] Panploo K., Chalermssinsuwan B., Poompradub S.: Natural rubber latex foam with particulate fillers for carbon dioxide adsorption and regeneration. *RSC Advances*, **9**, 28916–28923 (2019).
<https://doi.org/10.1039/C9RA06000F>
- [12] Kudori S. N. I., Ismail H.: The effects of filler contents and particle sizes on properties of green kenaf-filled natural rubber latex foam. *Cellular Polymers*, **39**, 57–68 (2019).
<https://doi.org/10.1177/0262489319890201>
- [13] Phomrak S., Nimpai boon A., Newby B. M., Phisalaphong M.: Natural rubber latex foam reinforced with micro- and nanofibrillated cellulose via dunlop method. *Polymers*, **12**, 1959 (2020).
<https://doi.org/10.3390/polym12091959>
- [14] Prasopdee T., Smitthipong W.: Effect of fillers on the recovery of rubber foam: From theory to applications. *Polymers*, **12**, 2745 (2020).
<https://doi.org/10.3390/polym12112745>
- [15] Karim A. F. A., Ismail H., Ariff Z. M.: Properties and characterization of kenaf-filled natural rubber latex foam. *BioResources*, **11**, 1080–1091 (2015).
<https://doi.org/10.15376/biores.11.1.1080-1091>
- [16] Eaves D.: *Handbook of polymer foams*. Rapra, Shrewsbury (2004).
- [17] Ramasamy S., Ismail H., Munusamy Y.: Tensile and morphological properties of rice husk powder filled natural rubber latex foam. *Polymer-Plastics Technology and Engineering*, **51**, 1524–1529 (2012).
<https://doi.org/10.1080/03602559.2012.715361>
- [18] Sirikulchaikij S., Kokoo R., Khangkhamano M.: Natural rubber latex foam production using air microbubbles: Microstructure and physical properties. *Materials Letters*, **260**, 126916 (2020).
<https://doi.org/10.1016/j.matlet.2019.126916>
- [19] Oliveira S.-L., Lopez-Gil A., Silva B.-F., Job A. E., Rodriguez-Perez M. A.: Natural rubber foams with anisotropic cellular structures: Mechanical properties and modeling. *Industrial Crops and Products*, **80**, 26–35 (2016).
<https://doi.org/10.1016/j.indcrop.2015.10.050>

- [20] Sukkaneewat B., Utara S.: Ultrasonic-assisted dunlop method for natural rubber latex foam production: Effects of irradiation time on morphology and physico-mechanical properties of the foam. *Ultrasonics Sonochemistry*, **82**, 105873 (2022).
<https://doi.org/10.1016/j.ultsonch.2021.105873>
- [21] Katkeaw K., Nooklay B., Kokoo R., Kooptarnond K., Khangkhamano M.: The Effect of nitrogen bubbles on microstructure of natural rubber foams produced by bubbling process. *Materials Science Forum*, **962**, 91–95 (2019).
<https://doi.org/10.4028/www.scientific.net/MSF.962.91>
- [22] Zhan Y., Hao S., Li Y., Santillo C., Zhang C., Sorrentino L., Lavorgna M., Xia H., Chen Z.: High sensitivity of multi-sensing materials based on reduced graphene oxide and natural rubber: The synergy between filler segregation and macro-porous morphology. *Composites Science and Technology*, **205**, 108689 (2021).
<https://doi.org/10.1016/j.compscitech.2021.108689>
- [23] Zhan Y., Oliviero M., Wang J., Sorrentino A., Buonocore G. G., Sorrentino L., Lavorgna M., Xia H., Iannace S.: Enhancing the EMI shielding of natural rubber-based supercritical CO₂ foams by exploiting their porous morphology and CNT segregated networks. *Nanoscale*, **11**, 1011–1020 (2019).
<https://doi.org/10.1039/C8NR07351A>
- [24] Zhan Y., Lavorgna M., Buonocore G., Xia H.: Enhancing electrical conductivity of rubber composites by constructing interconnected network of self-assembled graphene with latex mixing. *Journal of Materials Chemistry*, **22**, 10464–10468 (2012).
<https://doi.org/10.1039/C2JM31293J>
- [25] Zhan Y., Lago E., Santillo C., Del Rio Castillo A. E., Hao S., Buonocore G. G., Chen Z., Xia H., Lavorgna M., Bonaccorso F.: An anisotropic layer-by-layer carbon nanotube/boron nitride/rubber composite and its application in electromagnetic shielding. *Nanoscale*, **12**, 7782–7791 (2020).
<https://doi.org/10.1039/C9NR10672C>
- [26] Ramasamy S., Ismail H., Munusamy Y.: Soil burial, tensile properties, morphology, and biodegradability of (rice husk powder)-filled natural rubber latex foam. *Journal of Vinyl and Additive Technology*, **21**, 128–133 (2015).
<https://doi.org/10.1002/vnl.21389>
- [27] Promsung R., Nakaramontri Y., Uthaipan N., Kummerlöwe C., Johns J., Vennemann N., Kalkornsurapranee E.: Effects of protein contents in different natural rubber latex forms on the properties of natural rubber vulcanized with glutaraldehyde. *Express Polymer Letters*, **15**, 308–318 (2021).
<https://doi.org/10.3144/expresspolymlett.2021.27>
- [28] Dananjaya S. A., Somarathna Y. R., Karunanayake L., Siriwardena S.: Waste mica as filler for natural rubber latex foam composites. *Journal of Polymer Research*, **29**, 71 (2022).
<https://doi.org/10.1007/s10965-022-02930-w>
- [29] Zheng L., Li C., Zhang D., Guan G., Xiao Y., Wang D.: Multiblock copolymers composed of poly(butylene succinate) and poly(1,2-propylene succinate): Effect of molar ratio of diisocyanate to polyester-diols on cross-link densities, thermal properties, mechanical properties and biodegradability. *Polymer Degradation and Stability*, **95**, 1743–1750 (2010).
<https://doi.org/10.1016/j.polymdegradstab.2010.05.016>
- [30] Treloar L. R. G.: The physics of rubber elasticity. Oxford University Press, Oxford (1975).
- [31] Ariff Z. M., Zakaria Z., Tay L. H., Lee S. Y.: Effect of foaming temperature and rubber grades on properties of natural rubber foams. *Journal of Applied Polymer Science*, **107**, 2531–2538 (2008).
<https://doi.org/10.1002/app.27375>
- [32] Abd-El-Messieh S. L., El-Nashar D. E., Khafagi M. G.: Compatibility investigation of microwave irradiated acrylonitrile butadiene/ethylene propylene diene rubber blends. *Polymer-Plastics Technology and Engineering*, **43**, 135–158 (2004).
<https://doi.org/10.1081/PPT-120027468>
- [33] Wong K-F. V., Bhshkar T.: Transport properties of alumina nanofluids. in ‘2006 ASME International Mechanical Engineering Congress and Exposition, Chicago, USA’ 13282 (2008).
<https://doi.org/10.1115/IMECE2006-13282>
- [34] Raveshatian A., Fasihi M., Norouzbeigi R., Rasouli S.: Curing and thermal degradation reactions of nano-alumina filled natural rubber latex foams. *Thermochimica Acta*, **707**, 179108 (2022).
<https://doi.org/10.1016/j.tca.2021.179108>
- [35] Bland J. M., Altman D. G.: Statistics notes: Measurement error. *BMJ*, **312**, 1654 (1996).
<https://doi.org/10.1136/bmj.312.7047.1654>
- [36] Zabihi A., Fasihi M., Rasouli S.: Microstructural and physical properties of thermoplastic corn starch/polystyrene blend foams affected by different contents and combinations of plasticizers. *Journal of Polymers and the Environment*, in press (2022).
<https://doi.org/10.1007/s10924-021-02293-1>
- [37] Abdul Azam F. A., Royan N. R. R., Yuhana N. Y., Radzuhan N. A. M., Ahmad S., Sulong A. B.: Fabrication of porous recycled HDPE biocomposites foam: Effect of rice husk filler contents and surface treatments on the mechanical properties. *Polymers*, **12**, 475 (2020).
<https://doi.org/10.3390/polym12020475>
- [38] Tangpasuthadol V., Intasiri A., Nuntivanich D., Niyompanich N., Kiatkamjornwong S.: Silica-reinforced natural rubber prepared by the sol-gel process of ethoxysilanes in rubber latex. *Journal of Applied Polymer Science*, **109**, 424–433 (2008).
<https://doi.org/10.1002/app.28120>
- [39] Phomrak S., Phisalaphong M.: Lactic acid modified natural rubber-bacterial cellulose composites. *Applied Sciences*, **10**, 3583 (2020).
<https://doi.org/10.3390/app10103583>

- [40] Mohan T. P., Kuriakose J., Kanny K.: Effect of nanoclay reinforcement on structure, thermal and mechanical properties of natural rubber–styrene butadiene rubber (NR–SBR). *Journal of Industrial and Engineering Chemistry*, **17**, 264–270 (2011).
<https://doi.org/10.1016/j.jiec.2011.02.019>
- [41] Ramli R., Chai A. B., Ho J. H., Kamaruddin S., Rasdi F. R., De Focatiis D. S.: Specialty natural rubber latex foam: Foamability study and fabrication process. *Rubber Chemistry and Technology*, in press (2021).
<https://doi.org/10.5254/rct.21.78938>
- [42] Sood A. K., Ohdar R. K., Mahapatra S. S.: Experimental investigation and empirical modelling of FDM process for compressive strength improvement. *Journal of Advanced Research*, **3**, 81–90 (2012).
<https://doi.org/10.1016/j.jare.2011.05.001>
- [43] Candioti L. V., De Zan M. M., Cámara M. S., Goicoechea H. C.: Experimental design and multiple response optimization. Using the desirability function in analytical methods development. *Talanta*, **124**, 123–138 (2014).
<https://doi.org/10.1016/j.talanta.2014.01.034>